# High-Speed Plasmonic Modulator for Simultaneous C- and O-Band Modulation with Simplified Fabrication

**Andreas Messner[1*], Pascal A. Jud[1], Joel Winiger[1], Wofgang Heni[1,2], Benedikt Baeuerle[1,2], Marco Eppenberger[1], Ueli Koch[1], Christian Haffner[1,3], Huajun Xu[4], Delwin L. Elder[4], Larry R. Dalton[4], Ping Ma[1], Juerg Leuthold[1]**

[1]*ETH Zürich, Institute of Electromagnetic Fields (IEF), 8092 Zürich, Switzerland*
[2]*Polariton Technologies AG, 8038 Zürich, Switzerland*
[3] *Now with National Institute of Standards and Technology, Physical Measurement Laboratory, Gaithersburg, Maryland 20899, USA*
[4]*Department of Chemistry, University of Washington, Seattle, WA 98195-1700, USA*
**amessner@ethz.ch*

**Abstract:** A plasmonic modulator spanning both C- and O-band for dual-band data modulation up to 100 Gbit/s in one single device is presented. Fiber-to-fiber insertion loss can be as low as 11 dB.


## 1. Introduction

Plasmonic communication components, particularly electro-optical modulators [1-4] and photodetectors [5, 6] have recently gained a lot of research attention and are on the brink of commercialization. The plasmonic technology does not encounter substrate limitations, and is thus well suited for the integration with various platforms, such as silicon photonics [2] or even with a BiCMOS backend [7]. It can be functionalized with Pockels effect materials [2, 8] to provide modulation functionality, or with germanium for high-speed detection [5]. While vertically stacked plasmonic metal-insulator-metal (MIM) slot waveguides have been long known [9, 10], recent research has focused on horizontal plasmonic slots [1-5, 7, 8, 11], because they can be filled easily with a functional material of choice. However, the manufacturing of narrow slots with high aspect ratios is challenging.

Here, we present a plasmonic modulator concept that is based on vertically defined MIM slot waveguides, which are filled with an organic electro-optic (OEO) material [12]. The vertical integration alleviates the challenges of lateral slot structuring and does not impose limits on the aspect ratio of the waveguide. Additionally, the vertical MIM waveguides can benefit from the very high surface quality of plasmonic metal sheets [13], which helps with poling the OEO material and reducing the plasmonic losses. Both the plasmonic waveguide and metal fiber-to-slot grating couplers [14] have feature sizes larger than 300 nm and are fabricated in one single lithographic step, hence enabling reliable fabrication. The technology offers fiber-to-fiber insertion losses of 11 dB, large optical bandwidths spanning both the C- and O-band and high-speed data modulation up to 100 Gbit/s.

## 2. The vertically stacked plasmonic modulator

The vertically stacked plasmonic modulator represents a new plasmonic modulator geometry. The phase modulator, see Fig. 1a, consists of a plasmonic waveguide and two metal gratings that couple light directly to and from cores of a multicore fiber. Fig. 1b shows the cross-section of the device. The structured top metal layer and the essentially unstructured bottom electrode form a plasmonic slot waveguide, which is filled by OEO material [12]. A thin $TiO_2$ layer promotes the poling process and has no detrimental effects [15]. The electrical driving signal is applied between the top and bottom electrodes. The resulting electrical field in the active material changes its refractive index by means of the linear electro-optic effect (Pockels effect), causing a linear phase modulation. Fig. 1c shows simulations of the optical mode and the electrical driving field. Both fields overlap very well and are strongly confined to the active material, resulting in a strong modulation efficiency.

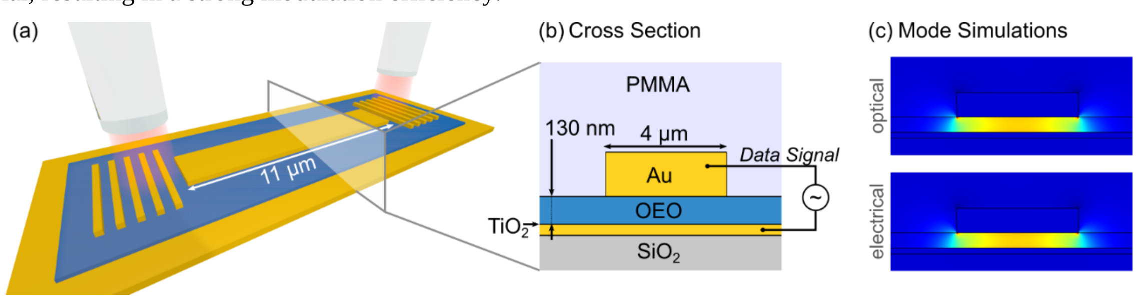


Fig. 1. (a) Schematic of the fabricated device with 11-um-long active section and input/output fiber cores. (b) Cross section through the MIM waveguide. (c) Mode simulations of the plasmonic (top) and RF electrical modes (bottom).

To fabricate the device, an optically thick gold layer was deposited by e-beam evaporation. The device is hence truly substrate-independent. Next, a 10-nm-thick $TiO_2$ was deposited by atomic layer deposition (ALD), and a 130-nm-thick OEO layer was applied by a spin coating process. After the evaporation of the solvent, 200 nm gold was evaporated to form the top metal layer. Structuring this layer defines all input and output couplers, together with the plasmonic waveguide. We used a negative-tone resist with e-beam lithography and a standard physical argon ion milling etching process. The identical input and output gratings consist of five equally spaced gold bars with a pitch of ~650 nm and a 50% filling factor. As the minimum feature size of the whole device is ~300 nm, a UV lithography system is well suited for the process, but was not available for fabrication of our devices. Finally, the chip was coated with PMMA and a poling process induced the OEO's nonlinearity.

In a first fabrication run, a passive proof-of-principle chip was fabricated using $SiO_xN_y$ ($n_{\mathrm{SiON}} = n_{\mathrm{OEO}}$@1550 nm) as a dielectric and a lift-off process for the structured gold film. Fig. 2a shows the measured fiber-to-fiber insertion loss of a device as shown in Fig. 1a with a 11-µm-long plasmonic waveguide. The grating's fiber-to-slot coupling efficiency is determined to be below 3 dB (note that the plasmonic waveguide itself breaks the symmetry of the grating, so that a CE better than -3 dB can be achieved). The transmission peaks at -11 dB and is only 1 dB below the insertion loss expected from simulation, which demonstrates the potential of future device generations.

Fig. 2b shows the measured fiber-to-fiber coupling spectra of the active device also used for the data modulation experiment described below. The measured fiber-to-fiber transmission is -20 dB both at 1310 nm and 1550 nm, with a transmission maximum of -16.5 dB at 1360 nm. The performance difference is attributed to roughness observable already during microscopy inspection and is not a fundamental limitation of the fabrication process.

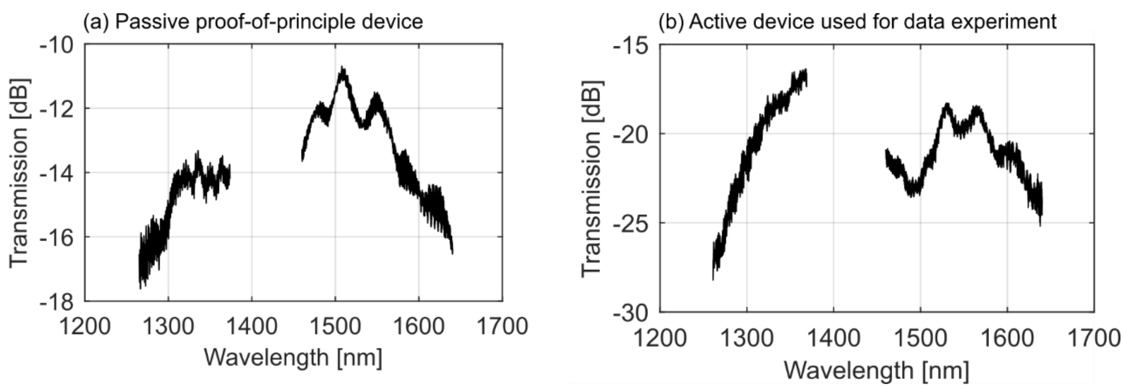


Fig. 2. Measured fiber-to-fiber transmission of the fabricated devices in the C- and O-band. (a) Fiber-to-fiber transmission of a passive, SiON-based proof-of-principle device. (b) Fiber-to-fiber transmission of the phase shifter used for the presented data modulation experiments

**3. Data Modulation Experiments**

Data modulation experiments have been carried out in the same phase shifter, both in the C- and O-band. A random bit sequence of length $2^{17}$ was generated offline and determined the non-return-to-zero on-off keying (NRZ-OOK) output signal of a digital-to-analog converter (DAC) at 100 GSa/s. The signal was electrically amplified and the voltage peak at the modulator was 2.6 $V_p$.

Fig. 3 shows schematic setup used for the data modulation experiments. Light from external cavity lasers at 1310 nm and 1550 nm was guided to a polarization controller before being fed to the chip. The incident optical power was 7-10 dBm. The modulated light was amplified by fiber amplifiers (erbium-doped for the C-band, praseodymium-doped for the O-band) and detected by an optical coherent receiver in a self-homodyne scheme. A real-time oscilloscope with an electrical bandwidth of 63 GHz sampled the signal with 160 GSa/s. After offline timing and carrier recovery, an LMS equalizer with 101 filter taps was applied. The reconstructed eye diagrams after equalization are shown in the inset of Fig. 3. Bit errors were counted after hard symbol decision, resulting in bit error ratios (BERs) of $6.17 \cdot 10^{-3}$ in the O-band and $5.7 \cdot 10^{-5}$ in the C-band have been measured. The performance limitation in the O-band lies in the available lab equipment designed for the C-band. Optical spectrum analysis and prior studies make clear that the devices actually work better around 1300 nm [16].

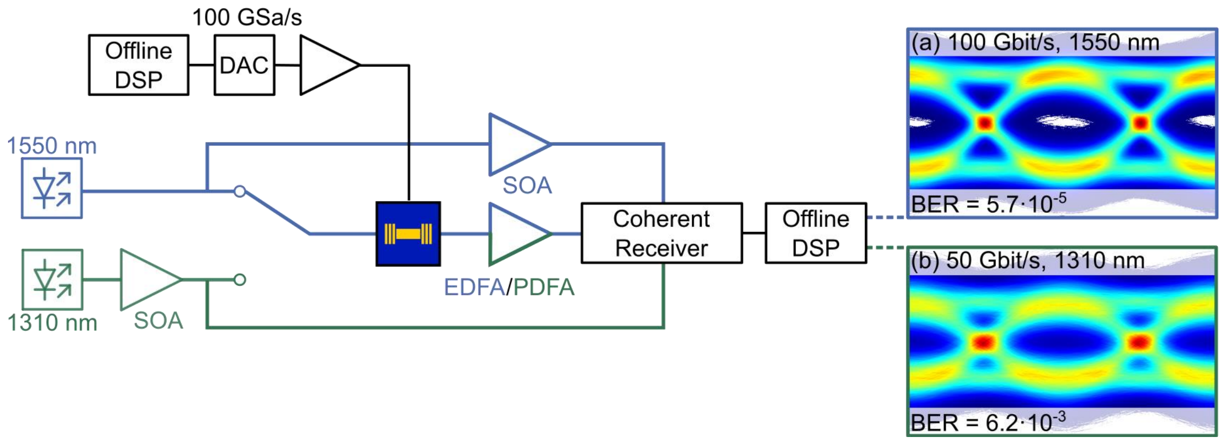


Fig. 3. Schematic of the data modulation experiment. Self-homodyne detection of 100 Gbit/s data modulation at 1550 nm and 50 Gbit/s at 1310 nm. Insets: Eye diagrams of (a) 100 Gbit/s data signal at 1550 nm, (b) 50 Gbit/s data signal at 1310 nm.

## 4. Conclusions

A plasmonic platform that combines broadband fiber-to-chip coupling with strong electro-optic modulation has been presented. For the first time, high-speed plasmonic modulators were fabricated with lithography steps requiring features no smaller than 300 nm. The gratings span both the C- and O-bands, with core-to-core transmission of -20 dB. Passive proof-of-principle devices feature a measured transmission of -11.5 dB, predicting further advantages in the technology. 100 Gbit/s (C-band) and 50 Gbit/s (O-band) NRZ OOK data modulation have been demonstrated in a single device, with BERs below been demonstrated in the C- and O-bands in a single device with BERs below and $5.7 \cdot 10^{-5}$ and $6.17 \cdot 10^{-3}$, respectively.

**Acknowledgements**

Financial support from the Swiss National Foundation under project 200021_159565 PADOMO and the Air Force Office of Scientific Research (FA9550-19-1-0069) is acknowledged.

## 5. References

[1] A. Melikyan *et al.*, "High-speed plasmonic phase modulators", *Nat. Photonics,* vol. 8, no. 3, pp. 229-233, 2014.
[2] C. Haffner *et al.*, "Plasmonic Organic Hybrid Modulators—Scaling Highest Speed Photonics to the Microscale", *Proc. IEEE,* vol. 104, no. 12, pp. 2362-2379, 2016.
[3] M. Burla *et al.*, "500 GHz plasmonic Mach-Zehnder modulator enabling sub-THz microwave photonics", *APL Photonics,* vol. 4, no. 5, p. 056106, 2019.
[4] W. Heni *et al.*, "Plasmonic IQ modulators with attojoule per bit electrical energy consumption", *Nature Communications,* vol. 10, no. 1, p. 1694, 2019.
[5] Y. Salamin *et al.*, "100 GHz Plasmonic Photodetector", *ACS Photonics,* vol. 5, no. 8, pp. 3291-3297, 2018.
[6] P. Ma *et al.*, "Plasmonically Enhanced Graphene Photodetector Featuring 100 Gbit/s Data Reception, High Responsivity, and Compact Size", *ACS Photonics,* vol. 6, no. 1, pp. 154-161, 2019.
[7] U. Koch *et al.*, "Monolithic High-Speed Transmitter Enabled by Bicmos-Plasmonic Platform," in *2019 European Conference on Optical Communication (ECOC)*, Dublin, 2019.
[8] A. Messner *et al.*, "Plasmonic Ferroelectric Modulators", *J. Light. Technol.,* vol. 37, no. 2, pp. 281-290, 2019.
[9] G. Veronis and S. Fan, "Theoretical investigation of compact couplers between dielectric slab waveguides and two-dimensional metal-dielectric-metal plasmonic waveguides", *Optics Express,* vol. 15, no. 3, pp. 1211-1211, 2007.
[10] R. Yang and Z. Lu, "Silicon-on-Insulator Platform for Integration of 3-D Nanoplasmonic Devices", *IEEE Photonics Technology Letters,* vol. 23, no. 22, pp. 1652-1654, 2011.
[11] G. Veronis and S. Fan, "Guided subwavelength plasmonic mode supported by a slot in a thin metal film", *Optics Letters,* vol. 30, no. 24, pp. 3359-3361, 2005.
[12] B. H. Robinson *et al.*, "Optimization of Plasmonic-Organic Hybrid Electro-Optics", *J. Light. Technol.,* vol. 36, no. 21, pp. 5036-5047, 2018.
[13] K. M. McPeak *et al.*, "Plasmonic Films Can Easily Be Better: Rules and Recipes", *ACS Photonics,* vol. 2, no. 3, pp. 326-333, 2015.
[14] M. Ayata, Y. Fedoryshyn, U. Koch, and J. Leuthold, "Compact, ultra-broadband plasmonic grating couplers", *Optics Express,* vol. 27, no. 21, pp. 29719-29729, 2019.
[15] W. Heni *et al.*, "Dielectric Layers in Plasmonic-Organic Hybrid Modulators," in *Advanced Photonics 2018 (BGPP, IPR, NP, NOMA, Sensors, Networks, SPPCom, SOF)*, Zurich, 2018, p. IW3B.3: Optical Society of America.
[16] C. Haffner *et al.*, "Harnessing nonlinearities near material absorption resonances for reducing losses in plasmonic modulators", *Optical Materials Express,* vol. 7, no. 7, 2017.